Electrical Engineering Faculty Articles   Electrical Engineering

7-17-2020

Controlling opto-electronic characteristics of ternary II–VI alloyed quantum dots: alcohol processing assay

Elaheh Kheirandish
University of Wisconsin-Milwaukee

J. Casey Marnocha
University of Wisconsin-Milwaukee

Nikolai Kouklin
University of Wisconsin-Milwaukee, nkouklin@uwm.edu

Follow this and additional works at: https://dc.uwm.edu/ceas_electrical-engineering_facart

PAPER • OPEN ACCESS

Controlling opto-electronic characteristics of ternary II–VI alloyed quantum dots: alcohol processing assay

View the article online for updates and enhancements.

Materials Research Express

PAPER

Controlling opto-electronic characteristics of ternary II–VI alloyed quantum dots: alcohol processing assay

E Kheirandish [ID] , J C Marnocha [ID] and N Kouklin [ID]

Department of Electrical Engineering and Computer Science, University of Wisconsin-Milwaukee, 3200 North Cramer St., Milwaukee, WI, 53211, United States of America

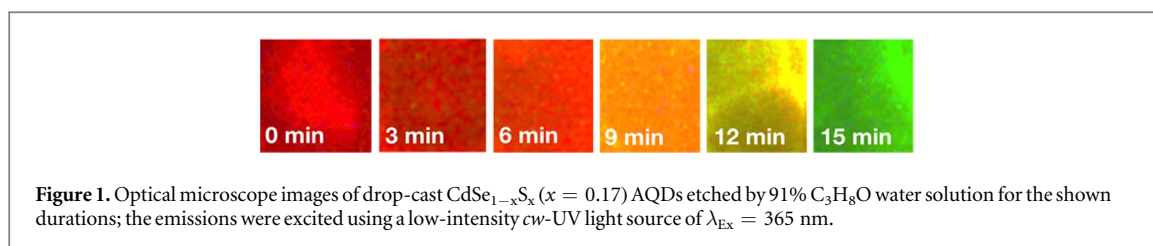E-mail: nkouklin@uwm.edu

Abstract

For their ultra-wide color gamut, high efficiency, robustness, and solution processability, Cd-based alloy semiconductor quantum dots (AQDs) continue to proliferate by driving innovations in the fields of optoelectronics, photovoltaics, multiplex bio-imaging, and cancer research. Herein, non-toxic, low-cost isopropyl alcohol vapor-based oxidative treatment protocol is developed and applied to tune the light emission spectrum of crystalline core–shell $CdSe_{1-x}S_x/ZnS$ quantum dots. As evidenced by the results of structural investigations, these AQDs when exposed to vapors produced ultrasonically from 10:1 isopropyl alcohol-to-water mix undergo an isotropic, diameter non-specific size reduction at the rate of $\sim$1.3 Å min^{-1}. Nonlinear time-dependent spectral shifts, revealed experimentally, are consistent with the results of the effective-mass approximation treatment. The emission yields are seen to undergo an initial drop, yet to plateau as the etch time increases. The study opens a door to a soft, top-down monotonic tailoring of the light emission characteristics and opto-electronic response of stoichiometrically- and hierarchically-complex core–shell constructs in technologically-viable group II–VI nano-semiconductors as well as AQD-based catalytic conversion of organic compounds.

Introduction

Semiconductor quantum dots (QDs), also known as artificial atoms, are quasi-zero-dimensional physical systems with an ultimate degree of charge carrier and exciton confinement and highly refined, size-tunable optoelectronic response. A recent progress pertaining to the controlled synthesis of colloidal binary core–shell QDs and the development of diverse surface-capping strategies have helped propel technological innovations across many fields including opto-electronics, bio-imaging, cancer research, and quantum communication to new heights [1–7]. In contrast to their elemental and binary counterparts [8], ternary semiconductor QDs and nanocrystals offer an additional degree of tunability of their light emission spectrum. These alloyed quantum dots (AQDs) possess many desirable characteristics such as increased external electroluminescent yield [9] as well as photovoltaic efficiency [10] that make them sought after for application in QD-based photo-detecting, energy harvesting, and light emitting devices [11–14].

Group II–VI semiconductor crystals and their alloy counterparts possess a range of key technologically-relevant opto-electronic responses and were a subject of detailed investigations before [15–18]. Among different ternary alloys, nanocrystal quantum dots in CdSeTe and CdSeS were studies most intensively as their band-edge emissions fall in the visible part of the electromagnetic spectrum [19]. While a hot-injection method remains a primary route to producing binary colloidal AQDs, other variants including diffusion based post-growth modification and non-injection one-pot approaches have been additionally developed to synthesize substrate-free AQDs [20, 21].

Yet, many challenges lie ahead and are stipulated by the inability to produce mono-disperse, size- and shape-specific AQDs while simultaneously maintaining their core stoichiometry. The problem is in-part associated

Figure 1. Optical microscope images of drop-cast $CdSe_{1-x}S_x$ ($x = 0.17$) AQDs etched by 91% C_3H_8O water solution for the shown durations; the emissions were excited using a low-intensity *cw*-UV light source of $\lambda_{Ex} = 365$ nm.

with overall fast, yet dissimilar reaction rates of chalcogenide precursors [22]. In addition, CdSeS spectral emission range can be practically tuned within a narrow window of ~125 nm.

To cover the entire visible range, i.e. ~400–650 nm, the alloy content has to be tuned in conjunction with the quantum dot physical size [23]. Unlike bulk semiconductors, whose dimensions can be altered using both additive and subtractive methods, owing to emission quenching by the surface defects/traps the top-down processing routes have to be ruled out for nano-semiconductors. Moreover, due to Ostwald ripening, synthesis of colloidal QDs with the size in a low nm-range is not feasible. Combined, this necessitates a search for and development of complimentary, yet soft and relatively fast etching protocols to tailor the size and, in turn, the opto-electronic response of stoichiometrically-complex nano-semiconductors including AQDs.

On this front, the dissolution of simpler, i.e. CdSe colloidal quantum dots were reported earlier in 3-amino-1-propanol/water mixtures [20] and in organic solvents by controlling precipitation-dissolution dynamics with surface stabilizing ligands [21]. The amine-assisted etching of CdSe remains very slow and time non-monotonic yielding highly anisotropic, pyramidally-shaped CdSe nanocrystals with Cd-terminated facets. [38] Faster etch rate, on the order of ~0.1 A min^{-1} were achieved with oleic acid [24]. Yet, the dissolution of CdSe was reported to be strongly size dependent with the size 'defocusing' and spectral broadening reported among the key drawbacks. As another drawback of amine-assisted etching, the temperature of the dissolution-growth reversal is to vary with the diameter which results in dissimilar QD size populations and undesirable color-splitting effects.

In this work, we develop and report a facile, i.e. one-step isotropic size-tuning of CdSeS/ZnS core–shell AQDs using an isopropyl alcohol/water based etching protocol. In contrast to other reported studies, the treatment is done in a vapor phase which obviates the need for AQD precipitation and re-suspension in the etch solutions. The vapor-treated AQD specimen are confirmed to retain their shape anisotropy and alloy content while remaining luminescent. The emission spectra are further found to exhibit a non-linear dependence on the etch time and the effects are successfully modeled/accounted for using the effective mass approximation framework as discussed below.

Processing methods

Vapor-based treatment

Highly-luminescent, ~6–8 nm diameter, oleic acid-capped $CdSe_{0.83}S_{0.17}$/ZnS core–shell AQDs suspended in toluene (~1 mg ml^{-1}) were obtained commercially (Sigma Aldrich). Their morphology, crystal structure and atomic compositions were obtained and the results are given below. As a first step, a 1 μl aliquot of AQDs is drop-cast onto a glass slide. Once toluene evaporated (~3–4 min) the slide was fitted vertically into a vial containing ~25 ml of C_3H_8O:H_2O solution (10:1) with AQDs located ~1 cm above the liquid/air interface.
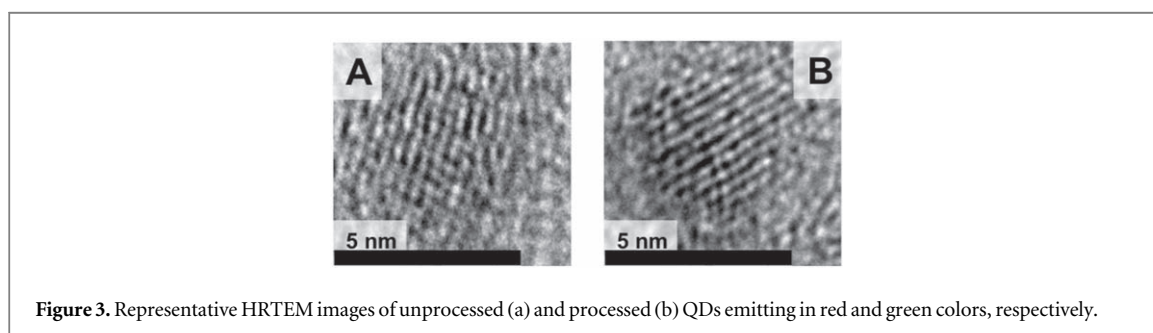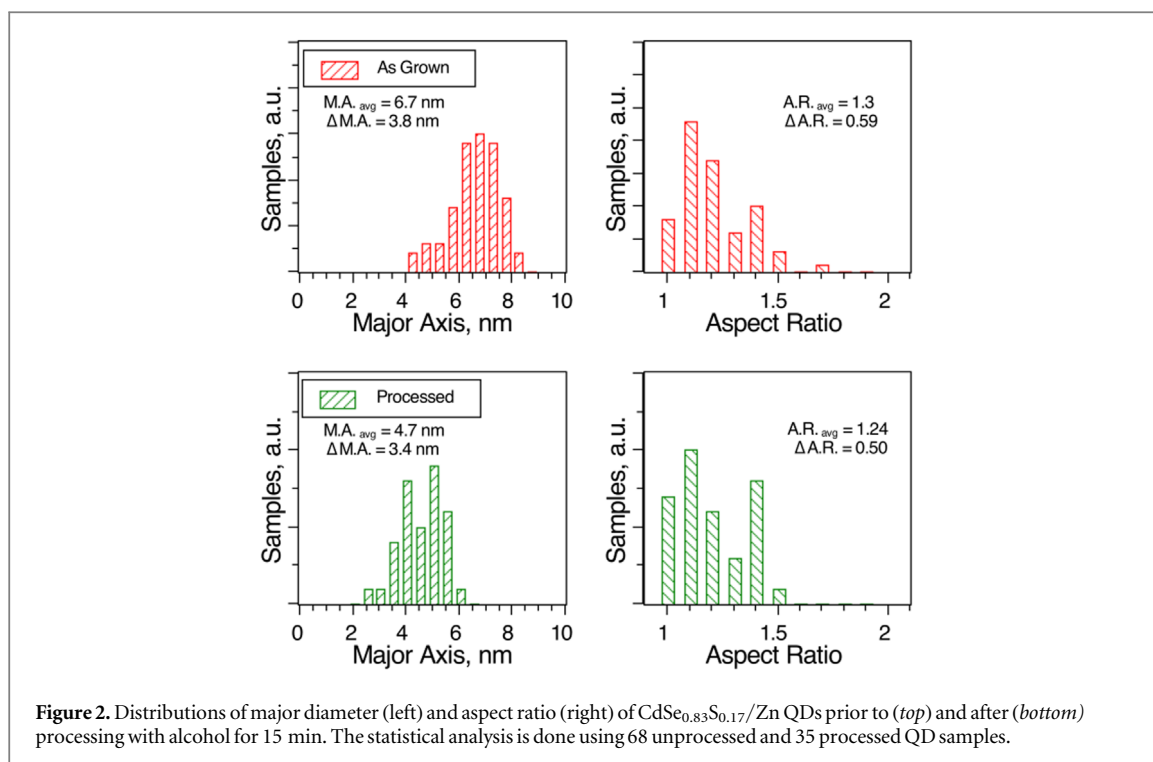
The solution was agitated and, in parallel, heated ultrasonically (Misonix 3000 with horn attachment, ~9 W power). The QD samples were exposed to the etchant mist/vapors using ~3 min time intervals for a total time of 15 min. At the end of each cycle, the slide was taken out to assess the spectral characteristics of QDs.

The emission spectrum of AQDs treated with ~10:1 isopropyl alcohol to DI water mixture exhibited a consistent blue-shift with the etch time, figure 1. Yet, treatments that were carried out similarly but only with either pure DI water or (~99.9%) C_3H_8O yielded no discernible change of the light emission characteristics. Longer exposures (>15 min) to ~99.9% pure C_3H_8O resulted in a noticeable reduction of the luminescence intensity.

Liquid phase treatment

Alternatively, the treatments were carried out in a liquid phase by drop-casting the same alcohol water solution directly onto AQDs whose temperature was maintained at ~60 °C with an external electrical (Joule) heater.

While the spectral trends (color shifts) were similar, the alternative pathway is found to be an order of magnitude slower compared to the sonication method. We attribute this to an increase in the oxygen levels and net higher local temperatures, the latter are likely to aid oleic acid cap removal thus speeding up the processing. A

Figure 2. Distributions of major diameter (left) and aspect ratio (right) of CdSe$_{0.83}$S$_{0.17}$/Zn QDs prior to (*top*) and after (*bottom*) processing with alcohol for 15 min. The statistical analysis is done using 68 unprocessed and 35 processed QD samples.

Figure 3. Representative HRTEM images of unprocessed (a) and processed (b) QDs emitting in red and green colors, respectively.

monotonic time-dependent blue-shift of the emission color of the AQDs is a primary indicator of the AQDs undergoing etching in the presence of the alcohol-water vapors. To verify the mechanism and to identify the chemical pathway, we carried out a set of the structural and optical property characterizations of the post processed AQDs, the results of which are presented and discussed next.

Results and analysis

We relied on HITACHI H-9000NAR High Resolution Transmission Electron Microscope (HRTEM) to assess the effect of the alcohol etching on the crystal order, morphology, size distribution, and aspect ratio of the AQDs comparatively, i.e. before and after the treatment. Figure 3 shows representative HRTEM images of as-received AQDs and the samples processed for 15 min. The electron diffraction patterns were additionally obtained and the results confirmed that the crystal structure of AQDs was similar to that of wurtzite bulk CdSe (supplementary materials is available online at stacks.iop.org/MRX/7/075008/mmedia), though the former possess slightly reduced lattice constants: $a = 4.12 \pm 0.32$ and $c = 6.72 \pm 0.04$ Å.

HRTEM images of larger ensembles of AQDs were collected to quantify the impact of the etch time on the diameter and aspect ratio distributions. According to figure 2, for the etch time of ∼15 min the major diameter shrank by ∼2.0 nm whereas the diameter aspect ratio changed by −4.6%, i.e. from 1.30 to 1.24, thus confirming that the alcohol etch rate remains isotropic.

The light emission characteristics of AQD samples were assessed next by carrying out room temperature *cw*-photoluminescence (PL) spectroscopic tests. The samples were excited with light generated by a 450 W Xenon lamp (excitation wavelength of ∼365 nm; optical power density of ∼5 mW cm^{-2}) and the emission spectra were collected with an Olympus 51X microscope and dispersed by another double-grating monochromator onto a
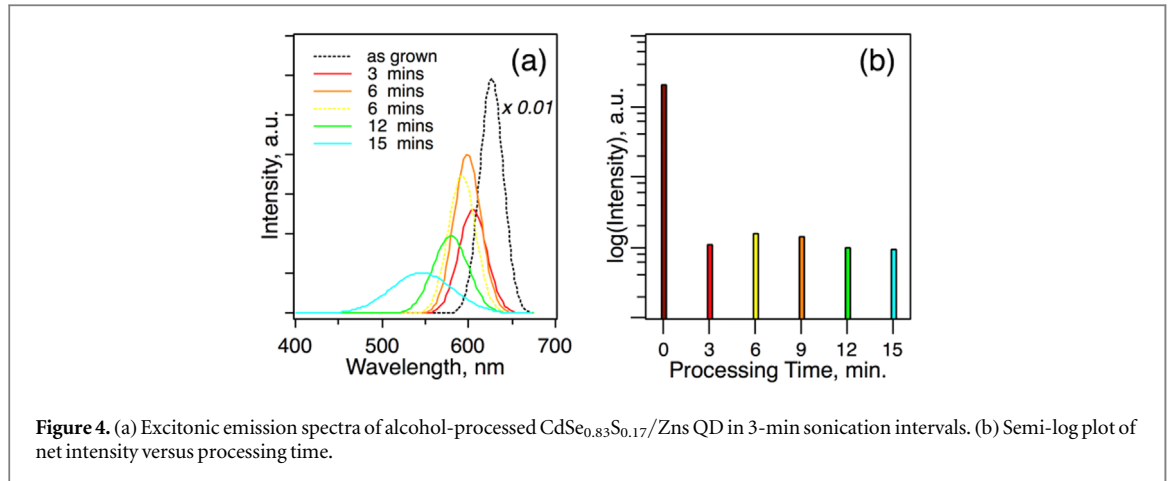
Figure 4. (a) Excitonic emission spectra of alcohol-processed CdSe$_{0.83}$S$_{0.17}$/Zns QD in 3-min sonication intervals. (b) Semi-log plot of net intensity versus processing time.

photomultiplier tube operating in a photon counting mode and serving as a detector. The instrument resolution was limited to 2 nm and the spectra were acquired in the range of ∼400–680 nm.

The emission spectra of the processed AQDs were obtained by Gaussian decomposition/fitting that helped identify and remove background PL that consisted of two static PL bands with peaks centered at ∼500 and 556 nm (supplementary materials) and attributed to the etch reaction by-products. The stand-alone individual narrow-width bands seen in figure 4(a) are excitonic emission bands of the AQDs. These AQD bands exhibit characteristic and very consistent blue shifting and slightly broaden as etch time increases. While initially the integral PL intensity decreases, it quickly stabilizes and remains almost unchanged for the treatment durations of up to 15 min, figure 4(b).

The observed initial drop of the quantum yield (QY) is generally expected as even a partial removal of the ZnS shell is to result in re-activation and increase of the ratio of the surface defects that act as non-radiative recombination centers [19, 25]. Assuming a typical shell thickness on the order of a monolayer, i.e. ∼3.1 Å for optimized core–shell QD configurations [25, 26] and the mean etch rate of ∼0.7 Å min^{-1}, etch time of ∼4 min should be sufficient to strip ZnS. The removal of the shell is to coincide with the onset of the non-radiative recombinations—a primary cause of the luminescence loss for semiconductor nano-crystals. In our case, the intensity loss is already evident at ∼3 min, figure 4(b) and attributed to a larger etch rate of the defect-prone ZnS shell. Furthermore, as the QD diameter reduces, the QY is to drop due to a rise of the surface-to-volume ratio.

Surface defects that act as PL quenches do play due to a large surface-to-volume ratio a more pronounced role in small diameter QDs, but only in uncapped ones. To our surprise and contrary to prior literature reports, the PL yields remain high for the treated samples as well. This is most likely due to the fact that etching recipe remains mild.

In contrast, the QY remained almost time-independent for etch durations >3 min, figure 4(b), in part due to an increase in the oscillator strength of the excitonic transitions in smaller size 0D systems.

The time-color interplay (figure 1) is next analyzed for bare AQDs (etch time >3 min) within the framework of effective mass approximation (EMA) [27, 28]. The band gap energy of bulk alloyed CdSe$_{1-x}$S$_x$ can be obtained based on the following equation,
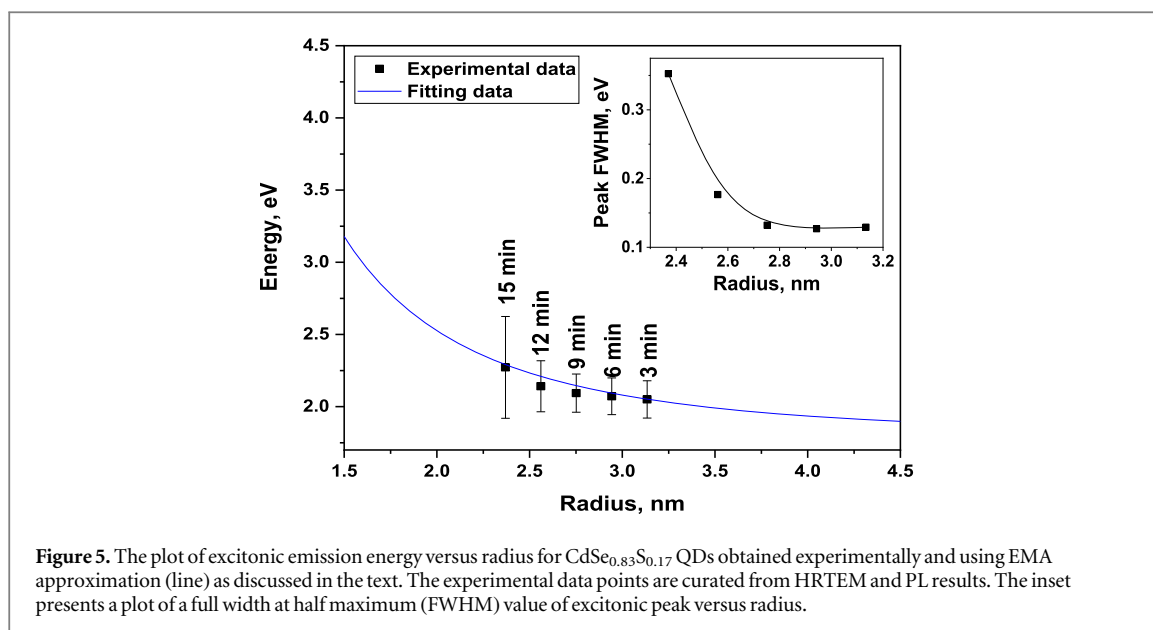
$$E_{g(CdSeS)} = (1 - x)E_{g(CdSe)} + xE_{g(CdS)} - bx(1 - x).$$

Using the bowing constant, $b = 0.28$ eV, EDX-retrieved elemental ratios of Cd:Se:S = 1:0.83:0.17, and the room temperature band gaps of CdSe and CdS of 1.74 and 2.42 eV, respectively, band gap of Cd$_1$Se$_{0.83}$S$_{0.17}$, E_g is estimated to be 1.81 eV [29]. The exciton Bohr radius can be estimated using $a_{B, AQD} \cong \epsilon_r \frac{m_0}{\mu} 0.053$ nm, where ϵ_r, m_0 and μ stand for dielectric constant, free electron and reduced masses, respectively, and is found to be ∼3.1 nm. Given the AQD radius, a is to be in the range of ∼2.3–3.1 nm $\leqslant a_{B, AQD}$, the confinement effects prevail and are to control spectral shifts. In this regime, the photon emission energy of the AQDs is obtained by treating Coulomb e-h interactions perturbatively, with the emission energy given by

$$E \approx E_{g_{CdSe_{0.83}S_{0.17}}} + \frac{h^2}{8a^2}\left(\frac{1}{m_e^*} + \frac{1}{m_h^*}\right) - \frac{1.8e^2}{4\pi \epsilon_{r_{CdSe_{0.83}S_{0.17}}} \epsilon_0 a}$$

where the second and third terms stand for the electron and hole confinement and Coulomb electrostatic potential energies, respectively. Approximating the electron and hole effective masses with their bulk values for CdSe: $m_e = 0.13m_0$ and $m_h = 0.45m_0$, and using $\epsilon_r = 6$ for Cd$_1$Se$_{0.83}$S$_{0.17}$ [30], we next obtain and plot the emission energy versus radius in figure 5.

Figure 5. The plot of excitonic emission energy versus radius for CdSe$_{0.83}$S$_{0.17}$ QDs obtained experimentally and using EMA approximation (line) as discussed in the text. The experimental data points are curated from HRTEM and PL results. The inset presents a plot of a full width at half maximum (FWHM) value of excitonic peak versus radius.
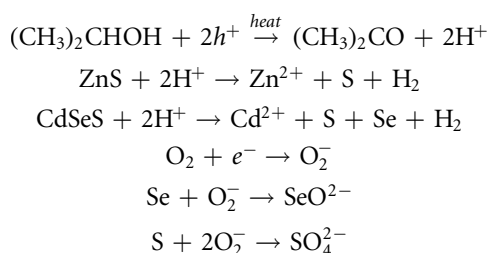
According to the results presented in figure 2, the size distribution, and, more specifically, diameter broadening is to vary only slightly with etching. Furthermore, as the temperature and, in turn, the net etch rate remain constant throughout the treatments, the radii of all AQDs are expected to shrink linearly with time. Given that the confinement energy prevails over the Coulomb energy (the last term in the above equation), both the spectral shift and the excitonic peak broadening are predicted to exhibit highly nonlinear time evolutions, which are readily evident in figure 5, the inset. This further serves as a confirmation that the light emission/ spectrum shifts are primarily controlled by the energy quantization effects in our AQDs with a mean diameter of up to ~7 nm. It should be noted that the results additionally point to a very negligible, if any, role of the radial alloy content gradient that can be present and induced by unbalanced precursor reactivities within the AQD cores [19, 21, 22].

The two background, i.e. ~500 and 556 nm PL peaks revealed by the Gaussian spectral decomposition only appear in the processed samples and therefore are attributed to the reaction by-products. The intensity and width of the 500 nm peak remain constant for all treatment durations, whereas the intensity of the 556 nm peak slightly increased with the processing time. The bands are consistent and assigned to a defect-associated luminescence originating from ZnO, CdS and CdO surface defect states, respectively. More specifically, the 500 nm emission involves oxygen vacancies of ZnO by-product. These oxygen vacancies are known to form deep-donor recombination states within the band gap of ZnO. The origin of the 556 nm band is traced to the surface defect states of CdS and CdO [31–34].

Oxidative degradation and etching of CdSe QDs could be linked to a molecular oxygen. Albeit possible, this pathway is to yield SeO$_2$, SO$_2$ and, more importantly, CdO as a surface capping layer. The latter is however to arrest the etch process, in contrast to what was observed by us experimentally. Since treatments with the water alone were equally ineffective, AQD etching pathways that involve water most likely are thermodynamically unfavorable [35].

Surprisingly, the AQD alcohol-based etching didn't proceed without water either. Due to an increased presence of defects, surface of Se-rich CdSeS is to carry a partial positive charge [36]. This is to render the AQD surface hydrophilic and to aid the surface absorption of water and, in turn, alcohol molecules from the mist. According to prior work [37], a surface-supplied positive charge, i.e. hole, h^+ is integral to photo-oxidation/ conversion of isopropyl alcohol into acetone which is accompanied by the formation of hydrogen radicals on CdS surface. Owing to a large surface-to-volume ratio and superior light absorption characteristics of spherically-shaped QDs, the latter mechanism can be particularly beneficial to both catalytic conversion of various organic compounds as well as etching of CdS nano-structures.

Depicted below are the key surface reactions that are likely, among others, to control the isopropyl alcohol etching of the core–shell AQDs in our case:

$$(CH_3)_2CHOH + 2h^+ \xrightarrow{heat} (CH_3)_2CO + 2H^+$$

$$ZnS + 2H^+ \rightarrow Zn^{2+} + S + H_2$$

$$CdSeS + 2H^+ \rightarrow Cd^{2+} + S + Se + H_2$$

$$O_2 + e^- \rightarrow O_2^-$$

$$Se + O_2^- \rightarrow SeO^{2-}$$

$$S + 2O_2^- \rightarrow SO_4^{2-}$$

In the above scheme, e^- and h^+ are either thermally or photo-generated ZnS- and CdS-supplied charges. The role of water is thus limited to assisting with (a) absorption of $(CH_3)_2CHOH$ and (b) removal of Zn^{2+}, Cd^{2+}, and SO_4^{2-} etch products. The metal cations are to eventually react with the oxygen and to precipitate as solid ZnO and CdO. It is worth noting that many secondary reactions such as those involving, for instance, S, Se and H while not shown, are not to be ruled out.

Summary

One-step, highly non-toxic and isotropic isopropyl-water based vapor etching protocol was developed and applied to continuously down-tune the size of highly heterogeneous $CdSe_{1-x}S_x/ZnS$ core–shell QDs. In contrast to many other, prior-developed top-down semiconductor processing routes, the composition and shape anisotropy of AQDs remain unaffected by the etching. The water is argued to play an important but mostly secondary role: a dissolution and removal of the reaction intermediates/by-products which will otherwise impede the etching. To restore emission yields, over-growth of ZnS or other similar cladding layer should be considered as a final post-etch step. The protocol can be used for precise tailoring of opto-electronic characteristics of group II–VI core–shell nano-semiconductors as well as AQD-based catalytic conversion of organic compounds.

Acknowledgments

Author contributions

E. K performed PL, EDX and HRTEM measurements, analyzed the results and helped edit the article. J. C. M performed treatment experiments, analysis of the size distributions and contributed to the article writing. N. K oversaw the studies, analysis and wrote the main article.

Additional information

The authors declare no competing interests.

ORCID iDs

E Kheirandish ⬤ https://orcid.org/0000-0001-5769-3504
J C Marnocha ⬤ https://orcid.org/0000-0002-7637-4493
N Kouklin ⬤ https://orcid.org/0000-0001-8244-3670

References

[1] Michler P, Kiraz A, Becher C, Schoenfeld W V, Petroff P M, Zhang L, Hu E and Imamoglu A 2000 A quantum dot single-photon turnstile device *Science* **290** 2282–5

[2] Bratschitsch R and Leitenstorfer A 2006 Artificial atoms for quantum optics *Nat. Mater.* **5** 855–6

[3] Wong C, Stylianopoulos T, Cui J, Martin J, Chauhan V P, Jiang W, Popović Z, Jain R K, Bawendi M G and Fukumura D 2011 Multistage Nanoparticle Delivery System for Deep Penetration into Tumor Tissue *Proc Natl Acad Sci U S A* **108** 2426–31

[4] Gao X, Cui Y, Levenson R M, Chung L W L and Nie S 2004 In vivo cancer targeting and imaging with semiconductor quantum dots *Nat. Biotechnol.* **22** 969–76

[5] Medintz I L, Uyeda H T, Goldman E R and Mattoussi H 2005 Quantum dot bioconjugates for imaging, labelling and sensing *Nat. Mater.* **4** 435–46

[6] Resch-Genger U, Grabolle M, Cavaliere-Jaricot S, Nitschke R and Nann T 2008 Quantum dots versus organic dyes as fluorescent labels *Nat. Methods* **5** 763–75

[7] Vardi A, Akopian N and Bahir G 2006 Room temperature demonstration of GaN／AlN quantum dot intraband infrared photodetector at fiber-optics communication wavelength *Appl. Phys. Lett.* **88** 143101

[8] Murray C B, Norris D J and Bawendi M G 1993 Synthesis and characterization of nearly monodisperse CdE (E = sulfur, selenium, tellurium) semiconductor nanocrystallites *J. Am. Chem. Soc.* **115** 8706–15

[9] Caruge J M, Halpert J E, Wood V, Bulović V and Bawendi M G 2008 Colloidal quantum-dot light-emitting diodes with metal-oxide charge transport layers *Nature Photon* **2** 247–50

[10] Ma W, Luther J M, Zheng H, Wu Y and Alivisatos A P 2009 Photovoltaic devices employing ternary PbS$_x$Se$_{1-x}$ nanocrystals *Nano Lett.* **9** 1699–703

[11] McDonald S A, Konstantatos G, Zhang S, Cyr P W, Klem E J D, Levina L and Sargent E H 2005 Solution-processed PbS quantum dot infrared photodetectors and photovoltaics *Nat. Mater.* **4** 138–42

[12] Kamat P V 2008 Quantum dot solar cells. Semiconductor nanocrystals as light harvesters *J. Phys. Chem.* C **112** 18737–53

[13] Demira H V, Nizamoglub B S, Erdemb T, Mutluguna E, Gaponikc B N and Eychmüller A 2011 Quantum dot integrated LEDs using photonic and excitonic color conversion *Nano Today* **6** 632–47

[14] Kamat P V 2013 Quantum dot solar cells. the next big thing in photovoltaics *J. Phys. Chem. Lett.* **4** 908–18

[15] Zhan Y, Shao Z, Jiang T, Ye J, Wu X, Zhang B, Ding K, Wu D and Jie J 2020 Cation exchange synthesis of two-dimensional vertical Cu$_2$S/CdS heterojunctions for photovoltaic device applications *J. Mater. Chem.* A **8** 789

[16] Shao Z, Jie J, Jiang T, Wu X, Li K, Xia F, Zhang X and Zhang X 2018 *Adv. Funct. Mater.* **28** 1706577

[17] Zheng N, Shao Z, Xia F, Jiang T, Wu X, Zhang X, Jie J and Zhang X 2017 One-step fabrication of CdS:Mo–CdMoO$_4$ core–shell nanoribbons for nonvolatile memory devices with high resistance switching *J. Mater. Chem.* C **5** 6156

[18] Liao W, Riutin M, Parak W J and Willner I 2016 Programmed pH-responsive microcapsules for the controlled release of CdSe/ZnS quantum dots *ACS Nano* **10** 1021

[19] Bailey R E and Nie S 2003 Alloyed semiconductor quantum dots: tuning the optical properties without changing the particle size *J. Am. Chem. Soc.* **125** 7100–6

[20] Zhao F and Kim J S 2012 Fabrication of CdSeS alloyed quantum dots and study on fluorescence lifetime *Mol. Cryst. Liq. Cryst.* **566** 120–5

[21] Ouyang J, Ratcliffe C I, Kingston D, Wilkinson B, Kuijper J, Wu X, Ripmeester J A and Yu K 2008 Gradiently alloyed Zn$_x$Cd$_{1-x}$S colloidal photoluminescent quantum dots synthesized via a noninjection one-pot approach *J. Phys. Chem.* C **112** 4908–19

[22] Smith D K, Luther J M, Semonin O E, Nozik A J and Beard M C 2010 Tuning the synthesis of ternary lead chalcogenide quantum dots by balancing precursor reactivity *ACS Nano* **5** 183–90

[23] Aubert T, Cirillo M, Flamee S, Van Deun R, Lange H, Thomsen C and Hens Z 2013 Homogeneously alloyed CdSe$_{1-x}$S$_x$ quantum dots (0 ⩽ x ⩽ 1): an efficient synthesis for full optical tunability *Chem. Mater.* **25** 2388–90

[24] Siy J T and Bartl M H 2010 Insights into reversible dissolution of colloidal CdSe nanocrystal quantum dots *Chem. Mater.* **22** 5973–82

[25] Dabbousi B O, Rodriguez-Viejo J, Mikulec F V, Heine J R, Mattoussi H, Ober R, Jensen K F and Bawendi M G 1997 (CdSe)ZnS core–shell quantum dots: synthesis and characterization of a size series of highly luminescent nanocrystallites *J. Phys. Chem.* B **101** 9463–75

[26] Steckel J S, Zimmer J P, Coe-Sullivan S, Bulovic V and Bawendi M G 2004 Blue Luminescence from (CdS)ZnS core–shell Nanocrystals *Angew. Chem. Int. Ed.* **43** 2154–8

[27] Efros A L and Rosen M 2000 The electronic structure of semiconductor nanocrystals *Annu. Rev. Mater. Res.* **30** 475–521

[28] Ekimov A I and Onushchenko A A 1981 Quantum size effect in three-dimensional microscopic semiconductor crystals *Journal of Experimental and Theoretical Physics Letters* **34** 345

[29] Wei S-H, Zhang S B and Zunger A 2000 First-principles calculation of band offsets, optical bowings, and defects in CdS, CdSe, CdTe, and their alloys *J. Appl. Phys.* **87** 1304–11

[30] Tripathy S K and Pattanaik A 2016 Optical and electronic properties of some binary semiconductors from energy gaps *Opt. Mater.* **53** 123–33

[31] Lin Y-J, Tsai C-L, Lu Y-M and Liu C-J 2006 Optical and electrical properties of undoped ZnO films *J. Appl. Phys.* **99** 093501–5

[32] Vasheghani Farahani S K, Muñoz-Sanjosé V, Zúñiga-Pérez J, McConville C F and Veal T D 2013 Temperature dependence of the direct bandgap and transport properties of CdO *Appl. Phys. Lett.* **102** 022102–5

[33] Katsaba A V, Ambrozevich S A, Vitukhnovsky A G, Fedyanin V V, Lobanov A N, Krivobok V S, Vasiliev R B and Samatov I G 2013 Surface states effect on photoluminescence of CdS colloidal nanocrystals *J. Appl. Phys.* **113** 184306

[34] Veamatahau A, Jiang B, Seifert T, Makuta S, Latham K, Kanehara M, Teranishid T and Tachibana Y 2015 Origin of surface trap states in CdS quantum dots: relationship between size dependent photoluminescence and sulfur vacancy trap states *Phys. Chem. Chem. Phys* **17** 2850

[35] Buxton G V, Greenstock C L, Helman W P and Ross A B 1988 Critical Review of rate constants for reactions of hydrated electrons, hydrogen atoms and hydroxyl radicals (OH/O⁻)in Aqueous Solution *J. Phys. Chem. Ref. Data* **17** 513–886

[36] Zeng Y and Kelley D 2017 Surface charging in CdSe quantum dots: IR and transient absorption spectroscopy *J. Phys. Chem.* C **121** 16657–64

[37] Nasalevich M A, Kozlova E A, Lyubina T P and Vorontsov A V 2012 Photocatalytic oxidation of ethanol and isopropanol vapors on cadmium sulfide *J. Catal.* **287** 138–48

[38] Li R, Lee J, Yang B, Horspool D N, Aindow M and Papadimitrakopoulos F 2005 Amine-assisted facetted etching of CdSe nanocrystals *J. Am. Chem. Soc.* **127** 2524–32